Development of a SPICE Model for Fabricated PLA/Al/Egg Albumin/Al Memristors Using Joglekar's Approach

Choudhury, Hirakjyoti ; Gogoi, Pallab Kr ; van der Knaap, R.; Goswami, Rupam ; Vanhamel , Jurgen

DOI
10.3390/electronics14050838

Publication date
2025

Document Version
Final published version

Published in
Electronics (Switzerland)

electronics

MDPI

Article

Development of a SPICE Model for Fabricated PLA/Al/Egg Albumin/Al Memristors Using Joglekar's Approach

Hirakjyoti Choudhury [1], Pallab Kr Gogoi [2,*], Ramon van der Knaap [3], Rupam Goswami [1] and Jurgen Vanhamel [2,4]

[1] Department of Electronics and Communication, Tezpur University, Tezpur 784028, India; ecp21108@tezu.ac.in (H.C.); rupam21@tezu.ac.in (R.G.)
[2] Space System Engineering, Delft University of Technology, 2629 HS Delft, The Netherlands; j.a.m.vanhamel@tudelft.nl
[3] Haagse Hogeschool, Rotterdamseweg 137, 2628 AL Delft, The Netherlands; 19149921@student.hhs.nl
[4] Electronic Circuits and Systems, KU Leuven, Kleinhoefstraat 4, 2440 Geel, Belgium
* Correspondence: p.k.g.gogoi@tudelft.nl

Abstract: Memristors have emerged as prospective two-terminal elements, having applications in memory, neuromorphic systems, and analog circuits. Biological materials such as egg albumin exhibit memristive behavior, displaying a distinctive pinched hysteresis signature in their current-voltage characteristics. However, such memristive behavior must be mathematically modeled to gain insights into the material's operation and utilize it in various circuit applications. This article proposes a novel SPICE-level framework for fabricated egg albumin memristors using Joglekar's memristor model. Experimental current-voltage characteristics are used to calibrate the SPICE model, ensuring accurate reproducibility of the experimental results. Additionally, the impact of variations in model-specific parameters on dynamic resistance and device performance is explored.

Keywords: memristor; egg albumin; SPICE; Joglekar's model; drop-cast

Academic Editor: Yahya M. Meziani

Received: 9 January 2025
Revised: 12 February 2025
Accepted: 17 February 2025
Published: 20 February 2025

Citation: Choudhury, H.; Gogoi, P.K.; Knaap, R.v.d.; Goswami, R.; Vanhamel, J. Development of a SPICE Model for Fabricated PLA/Al/Egg Albumin/Al Memristors Using Joglekar's Approach. *Electronics* **2025**, *14*, 838. https://doi.org/10.3390/electronics14050838

1. Introduction

CMOS technology is fast approaching its fundamental limitations with the growing demand for miniaturization. Excessive heat dissipation and increasing fabrication cost are primary concerns as the transistor density on the chip increases [1]. The memory problem where the memory latency and bandwidth become insufficient for instruction and data transfer to a processor is also more prominent with the ever-increasing amount of data computations using conventional microelectronics technology [2]. Conventional memory technologies such as Flash, DRAM, and SRAM are not able to keep up with the demand for scaling and low power.

Similarly, several studies have explored advancements in non-volatile memory technologies, focusing on improving efficiency, reliability, and integration with modern computing architectures. Mohammad et al. introduced an efficient and compact Fe-CNTFET-based ST using only two transistors. The hysteretic behavior of Fe-CNTFETs enables an auto-non-volatile structure, eliminating the need for additional non-volatile components. To demonstrate its practical applications, two auto-non-volatile latches were shown to enhance the soft error tolerance of traditional ST-based latches [3].

Traditional CMOS-based methods often suffer from high energy consumption and large circuit footprints. Addressing this, researchers utilized two crossbar arrays of ferroelectric FinFETs to compute the Mahalanobis distance, a key metric for outlier detection in

correlated data. When tested on the Wisconsin breast cancer dataset, the design achieved 94.1% accuracy while consuming only 13.56 picojoules, highlighting its efficiency in complex data analysis [4].

Additionally, Xiu-Lan Cheng et al. explored Ga-doped phase change memory (PCM) as a next-generation non-volatile memory candidate. Their study focused on the unique data storage mechanism of PCM, particularly for sub-65 nm technologies. Their simulations demonstrated methods to enhance Ga-doped PCM's performance and reliability for embedded non-volatile memory applications [5].

Berdan et al. developed a SPICE-compatible model for resistive random-access memory (ReRAM) that accounts for state drift and resistance degradation over time—challenges often overlooked in idealized models. By incorporating the physical mechanisms of resistive switching, their model enables realistic simulations, improving circuit design and performance predictions for memory storage and neuromorphic computing applications [6].

In contrast to conventional metal–oxide ReRAM, GIG-based ReRAM eliminates the need for an initial forming process, simplifying circuit integration. Researchers developed a physics-based model incorporating key switching mechanisms, demonstrating that GIG ReRAM offers improved performance and lower power consumption, making it a strong candidate for next-generation non-volatile memory and neuromorphic computing [7].

Memristors, an upcoming nanoscale technology, have the ability to address these difficulties [8]. In 1971, Leon Chua predicted the existence of a fourth fundamental element (the other three are resistor, capacitor, and inductor) known as the memristor (memory with resistor) [9]. Following Chua's conceptualization, HP Labs fabricated the first TiO_2-based memristor in 2008, which consisted of a titanium dioxide (TiO_2) layer sandwiched between two platinum electrodes [10].

On the other hand, protein is a natural material with interesting electrical properties. It has been utilized to create field-effect transistors (FETs), memristors (resistive switching devices), non-volatile memory devices, and lab-on-chip architectures. Egg albumin is biodegradable, bioresorbable, and ecologically friendly, making it a promising material for electronic applications. Egg albumen has been employed as an active or dielectric layer to create high-performing thin-film transistors and resistive switching devices. It has also been utilized to increase ultraviolet (UV) fluorescence by adding Au nanoparticles. Although there has been progress, more effort is still required to improve the performance, stability, and dependability of egg albumin-based memristor devices and to clarify the functioning mechanics. To provide full electronic functionalities, further device and operation types are required for future applications [11].

Interestingly, various biological samples exhibit memristive behavior. Organic materials such as sweat ducts, the Mimosa pudica plant, Dionaea muscipula (Venus flytrap), and amoebas have demonstrated characteristics akin to memristors, as described by Chua [12–14]. Sueoka et al. investigated neural facilitation in a honey-based organic synaptic memristor [15–17], while Gale et al. observed memristive properties in the protoplasmic tubes of Physarum polycephalum [18]. Additionally, Johnsen et al. reported that human sweat ducts exhibit memristor-like behavior [19]. Hota et al. successfully synthesized transparent memristors using silk fibroin protein derived from Bombyx mori silkworm cocoons [20].

Egg albumin has also been explored as a bio-material for memristor fabrication due to its inherent dielectric properties. Memristor devices leveraging egg albumin have potential applications in non-volatile memory storage and neuromorphic computing, where synaptic processes are mimicked to develop advanced neural network-inspired systems. The fabrication process typically involves preparing a uniform egg albumin dielectric layer, integrating aluminum (Al) electrodes, and constructing a memristor structure such as Al/egg albumin/Al. The memristive behavior is validated through electrical characteriza-

tion, particularly current–voltage (I–V) measurements, to assess hysteresis and switching dynamics. These findings highlight the potential of egg albumin-based memristors for bio-inspired computing and memory applications.

Egg albumin-based bio-memristors offer numerous advantages, including a simple structure, scalability, potentially low cost, and low power consumption [21,22]. However, concerns remain regarding the environmental and health impacts of toxic organic materials often used in these devices. To address these issues, researchers have been actively investigating non-toxic bio-material alternatives for the past two decades. Egg albumin, being biodegradable, biocompatible, and environmentally friendly, has emerged as a promising candidate [23]. Protein-based materials have already been successfully employed to fabricate bio-memristors [24].

Despite significant advancements, further research is necessary to fully understand the electrical properties of bio-memristors, as their behavior remains somewhat ambiguous. Given their adaptability and relevance in electronic applications, SPICE (Simulation Program with Integrated Circuit Emphasis) models are widely used to evaluate fundamental memristor models, facilitating further development [25]. SPICE models play a crucial role in the modeling and design of novel electronic devices, enabling engineers to predict and analyze circuit behavior before actual implementation. By allowing parameter modifications, these models offer flexibility in developing emerging technologies such as memristors, supporting the simulation of device behavior under various conditions. This capability aids in designing memristor-based circuits, including neural networks and memory arrays, before fabrication [26].

The SPICE memristor model enables adjustments to the I–V characteristics through modifications of various parameters. Given the diversity in memristor compositions and structures, multiple SPICE modeling techniques have been developed. Several compact SPICE models have been introduced to replicate the behavior of existing memristor devices, and numerous subcircuits have been designed to simulate memristors in SPICE simulations [27].

While these models align well with experimental data for sinusoidal inputs, they exhibit deviations for intermediate-resistance states. Since the inception of memristor devices, numerous SPICE models have been proposed, each employing a state-variable equation to determine dynamic resistance [28]. The dynamic resistance is inversely proportional to the physical properties of the memristor, which are reflected in the value of the state variable. Consequently, the state-variable equation can be utilized to determine various I–V characteristics [29].

In this context, the Joglekar model is widely used in memristor research due to its simplicity, computational efficiency, and ease of implementation. One of its key advantages is the window function, which ensures that the state variable remains within physical limits, preventing unrealistic growth beyond the thickness of the memristor. This feature makes the model particularly valuable for theoretical studies and circuit simulations, providing a smooth transition between different resistance states that aligns well with real-world memristive behavior. Additionally, the model can be adapted to various memristor devices by adjusting parameters such as mobility and charge-dependent dynamics, further enhancing its applicability [30].

In comparison to other memristor models, the Joglekar model is often preferred for foundational and theoretical research. While the Yakopcic model introduces voltage-dependent switching for greater physical realism, and the Biolek model improves boundary handling, these enhancements come with increased complexity. The Joglekar model, on the other hand, offers a tunable nonlinearity parameter that allows flexible variation of memristor behavior while maintaining a simplified structure. This makes it ideal for

preliminary investigations where computational efficiency is prioritized over detailed hardware modeling [31,32].

Although the Biolek and Yakopcic models provide improved accuracy near state boundaries, the Joglekar model remains a popular choice in SPICE simulations and analytical studies due to its ease of implementation. For applications that do not require extensive physical constraints, it presents an efficient and practical approach to memristor modeling [31,32].

This paper focuses on the fabrication and characterization of a bio-memristor using egg albumin as the memristive material. The material exhibits resistive behavior, and the experimental I–V curves fit well with existing memristor models. A SPICE-level implementation of drop-cast PLA/Al/egg albumin/Al memristors is described in this paper.

The primary contributions of this article are as follows:

- The Joglekar memristor model is used to build egg albumin memristors at the SPICE level. The model's parameters are adjusted based on the parameters that are taken from the experimental data.
- Discussing and summarizing the effects of altering the various SPICE model parameters.
- Understanding how important parameters affect the hysteresis loop. Therefore, a set of parameters is presented to describe quantification of the hysteresis loops in the I–V plane.

The rest of the paper is organized as follows: Section 2 details the fabrication process and electrical characterization of the egg albumin memristors. Section 3 introduces a SPICE-level structural model for the memristors, and the results are comprehensively discussed in Section 4. Finally, the conclusions are presented in Section 5.

2. Fabrication and Electrical Characterization of PLA/Al/Egg Albumin/Al Memristor

This section briefly describes the methodology used to fabricate drop-cast egg albumin memristors on 3D-printed substrates.

2.1. Fabrication Process

The fabrication process of the egg albumin memristor involved several steps. In **step A**, 10 mL of chicken egg albumin was extracted from the egg yolk using a dropper and a strainer. In **step B**, a rectangular substrate with dimensions 27×15 mm^2 and a thickness of 2 mm was fabricated using EN-PLA material and a 3D printer (Model No. Ender 1200P). The substrate was then cleaned with deionized water after printing. The active area of the memristor was coated with chicken egg albumin using a drop-casting process.

An aluminum electrode with dimensions 48×8 mm^2 and a thickness of 0.15 mm was used, with the electrode gap in the active region set to 0.5 mm. The egg albumin, possessing memristive properties, was deposited on the active region of the bio-memristor using a dropper, and the sample was dried at room temperature (300 K) for further analysis. Figure 1A,B illustrate the methodology.

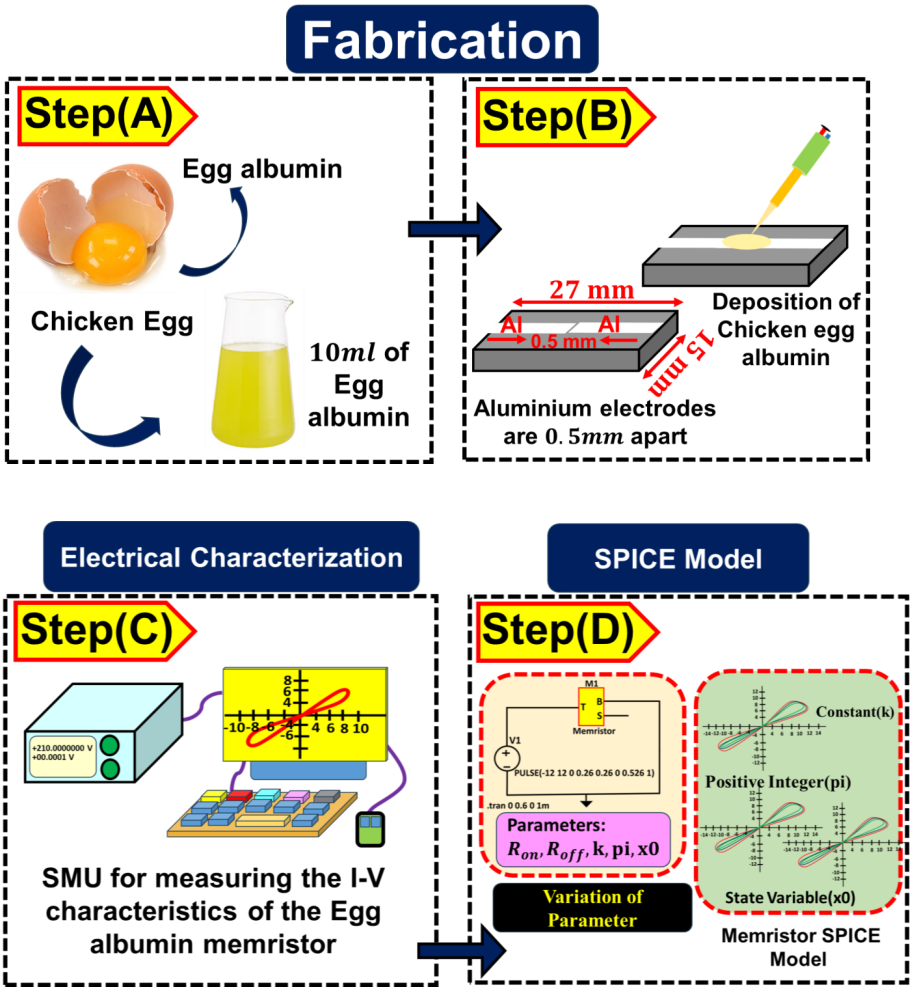

Figure 1. Workflow showing the methodology: (**A**) egg albumin extraction; (**B**) deposition of chicken egg albumin on the 3D-printed substrate; (**C**) electrical characterization; (**D**) SPICE model.

2.2. Electrical Characterization

In **step C**, the I−V characteristics of the egg albumin memristor were measured using a source measurement unit (SMU). Finally, in **step D**, a memristor subcircuit with parameter variations was implemented to analyze the device's performance. Figure 1C,D illustrate the methodology. The electrical characterization of the egg albumin bio-memristor was performed using an SMU, with all measurements conducted at room temperature.

The current–voltage (I−V) characteristics of the fabricated bio-memristor are presented in Figure 2a, where the arrows indicate the sweep direction of the applied voltage, ranging from −12 V to +12 V. A switching ratio of 0.26 was observed within the pinched hysteresis loop. For the positive half-cycle, the loop exhibited minimum and maximum currents of 0.4 mA and 10 mA, respectively, while for the negative half-cycle, the minimum and maximum currents were 0.244 mA and 9.69 mA, as illustrated in Figure 2b. Table 1 presents a comparative analysis of the switching ratio of the proposed memristor with other bio-based memristors. Readers can refer to Supplementary Materials provided in this work for more details.

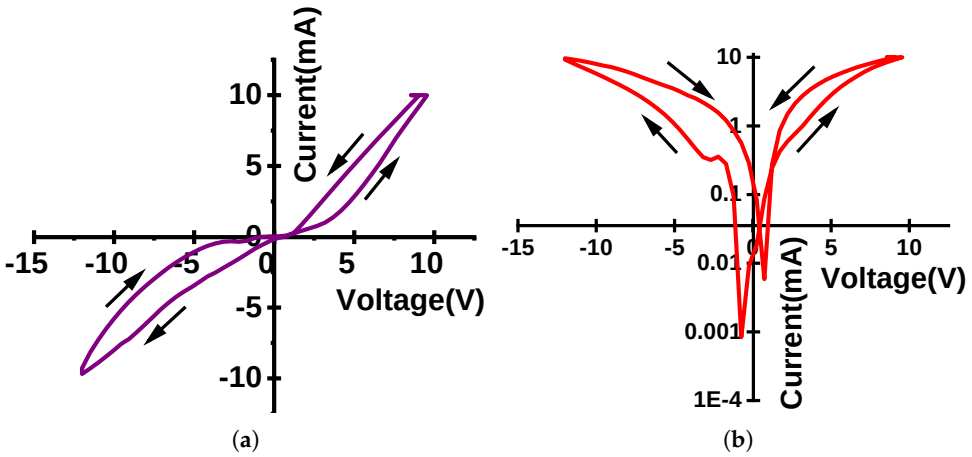

Figure 2. Measured I−V characteristics for egg albumin memristors on (**a**) linear scale and (**b**) logarithmic scale.

Table 1. Different types of memristors for bio−materials and their switching ratios.

Ref.	Bio-Material	Method	r_{on}, r_{off}	$\frac{r_{on}}{r_{off}}$
[33]	Sweat ducts in the skin	Dry disc electrodes	360 kΩ, 417 kΩ	0.86
[34]	Leaf of aloe vera	Identical (Pt or Ag/AgCl) electrodes for measuring and as reference (Ref)	218 kΩ, 321 kΩ	0.67
[35]	Potato tubers	Teflon-coated platinum wires with a 0.076 mm diameter and AgCl electrodes for measurement and reference (Ref) in every experiment	2042 kΩ, 6060 kΩ	0.33
[36]	Pumpkin seeds	Platinum Electrode Based Measurement	393 kΩ, 419 kΩ	0.93
[37]	Protein blend	Liquid Sample Holder in a Potential Divider Arrangement	0.4 kΩ, 1.112 kΩ	0.35
[21]	Egg albumin	Deposition Using Spin Coating	0.06 kΩ, 99.2 kΩ	6×10^{-4}
[38]	$BiFeO_3$ @egg albumen nanocomposite	Deposition Using Spin Coating	0.073 kΩ, 0.181 kΩ	4×10^{-1}
This work	Egg albumin	Drop-casting is used to deposit egg albumin into PLA substrate	0.782 kΩ, 2.899 kΩ	0.26

3. SPICE-Level Framework for Proposed Memristors

This section presents a detailed description of the SPICE-level framework for the egg albumin memristors, along with the steps for parametric extraction from the experimental characteristics.

3.1. SPICE Models

3.1.1. Joglekar Model

The Joglekar model is a mathematical model that describes the behavior of memristors. It includes a window function to manage state-variable evolution and avoid uncontrolled expansion. The change in the state variable x (which influences memristance) is represented as

$$\frac{dx}{dt} = kI(t)f(x) \tag{1}$$

where x is the normalized state variable ($0 \leq x \leq 1$), k is a scaling constant controlling the switching speed, and $I(t)$ is the applied current.

In the Joglekar model, the window function is defined as

$$f(x) = 1 - (2x - 1)^{2pi} \tag{2}$$

where pi is a positive integer that affects the function's shape and x is the normalized state variable, which ranges from 0 to 1 [30].

3.1.2. Knowm Memristor Model

The Knowm Memristor Model, particularly the Generalized Metastable Switch (MSS) model, is intended to accurately represent the behavior of various memristive devices. The model defines a state variable x to reflect the device's metastable-state occupancy probability. The evolution of x over time is governed by

$$\frac{dx}{dt} = f(x, V, T) \tag{3}$$

where V is the applied voltage, T is the temperature, and f describes the rate of change of x based on the device's physical properties and external conditions.

The current passing through the memristor is given by

$$I = g(x, V, T) \tag{4}$$

where the function g simulates the device's conductance based on the state variable x, applied voltage V, and temperature T [39].

3.1.3. Biolek Memristor Model

The Biolek memristor model enhances comprehension of memristive behavior by integrating nonlinear dopant drift and an asymmetric window function. This approach more accurately represents real-world memristor dynamics, particularly near the device boundaries.

The rate of change of the state variable w is given by

$$\frac{dw}{dt} = \mu_v \frac{r_{on}}{D} I(t) f(w, I) \tag{5}$$

where μ_v is the mobility of dopants, r_{on} is the low resistance state, D is the thickness of the memristive layer, $I(t)$ is the applied current, and $f(w, I)$ is the Biolek window function.

The window function, which influences the development of the state variable, especially at its boundaries, is defined as

$$f(w, I) = 1 - |w - \text{sgn}(I)|^{2p} \tag{6}$$

where w is the normalized state variable ($0 \leq w \leq 1$), $\text{sgn}(I)$ is the sign function of the current, and p is a positive integer controlling the window's sharpness [40].

3.2. Joglekar Memristor Model and SPICE Subcircuit

The Joglekar memristor model serves as a foundational framework for memristor research, yet it exhibits significant limitations that constrain its applicability to real-world devices. One major drawback is its reliance on a symmetric window function, which fails to accurately capture the asymmetric switching behavior observed in many memristors. This symmetry can introduce errors when modeling a device's response to varying voltage polarities. Additionally, the window function flattens near the state variable's boundaries, causing the state to approach its limits too slowly. This characteristic poses challenges in modeling memristors with abrupt resistance transitions between high and low states [41].

Organic memristive devices can be simulated using the Joglekar memristor model because it can capture the special properties of these materials. When it comes to resistive switching, organic memristors frequently display nonlinear ion drift and boundary effects. These problems are addressed by the Joglekar model by introducing a window function that modifies the development of the state variable. The Joglekar model is an important and simple tool for researchers investigating and building organic memristive systems because it makes it possible to replicate the slow resistance changes and hysteresis seen in organic structures [42].

Ascoli et al. discuss the difficulties in modeling circuits based on memristors. Memristors are nonlinear two-terminal devices with complicated dynamical behaviors that can cause numerical errors and convergence problems when their governing differential-algebraic equations undergo computer-aided integration. The authors provide a strategy that entails reformulating the initial differential-algebraic equation sets into an ongoing and differentiable form in order to avoid these difficulties. This reformulation ensures well-behaved numerical solutions while faithfully capturing the dynamics of the original memristor model. The altered set of equations is made to operate with commercial circuit simulators, making it easier to incorporate into current design processes [43].

The primary mechanism behind multi-level switching in these devices is attributed to the trapping and de-trapping of charge carriers [37]. Chen et al. fabricated and characterized non-volatile resistive switching memory devices using unprocessed chicken egg albumen as a dielectric layer. Low-frequency noise (LFN) measurements, commonly used to analyze conduction mechanisms, fluctuation sources, and defect states in electronic devices, revealed that carrier trapping and de-trapping phenomena significantly influence noise behavior. Chen et al. also observed that electron capture and emission within conductive filaments dominate the current transport mechanism in albumen-based resistive switching devices, as indicated by the measured 1/f noise characteristics [21].

The experimental I–V properties of egg albumin memristors are modeled using the Joglekar memristor model [30]. Table 2 lists the equations of the Joglekar memristor model along with their explanations. A bio-memristor within the SPICE framework can be represented by varying several parameters derived from the mathematical expressions of the Joglekar memristor model.

The Appendix A provides the SPICE model. The starting state variable (S) is represented by a terminal, as depicted in Figure 3a, where the top electrode (T) and bottom electrode (B) serve as terminals for applying voltage across the memristor [44].

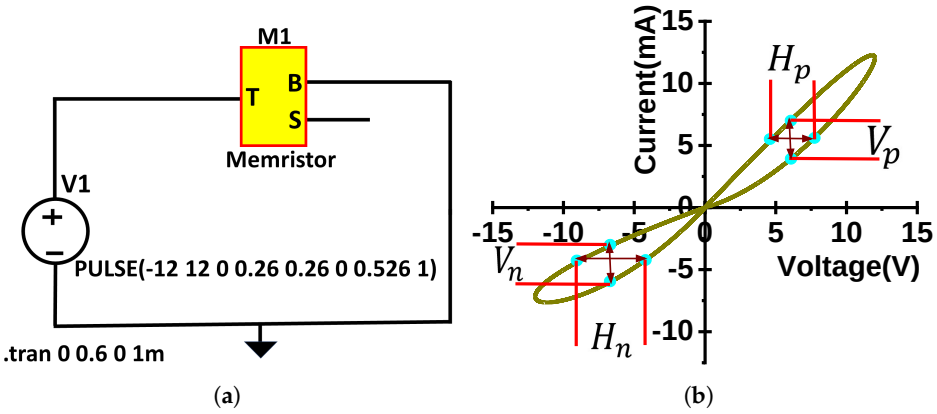

Figure 3. (**a**) Structure of memristor SPICE circuit [44] and (**b**) schematic showing extraction of V_p, H_p,V_n, and H_n.

Table 2. Joglekar memristor model equations and their description [30].

Joglekar Memristor Model Equation	Physical Quantities	Description
$C_{\text{int}} \cdot \frac{dS}{dt} = I(t)$	C_{int} = capacitance; $\frac{dS}{dt}$ = rate of change of state variables; $I(t)$ = current	Initial condition of a capacitor representing internal capacitance.
$V(S(0)) = x_0$	$V(S)$ = voltage; $V(S(0))$ = initial state variable; x_0 = initial condition	Initial condition for voltage, where x_0 is the initial state.
$G_s(0,S) = \left\{ \frac{k \cdot V(T,B)}{r_{\text{on}} \cdot V(S) + r_{\text{off}} \cdot (1 - V(S))} \times \left[1 - (2 \cdot V(S) - 1)^{2pi}\right] \right\}$	G_S = current source; k = constant; $V(T,B)$ = voltage across memristor; $V(S)$ = state variable; r_{on} = low resistance; r_{off} = high resistance; pi = Joglekar window parameter	Equation defining G_s0S, incorporating linear and nonlinear components of the memristor model.
$G_1(T,B) = V(T,B) \cdot \left[\frac{1}{r_{\text{on}} \cdot V(S) + r_{\text{off}} \cdot (1 - V(S))}\right]$	$G_1(T,B)$ = current through memristor; $V(T,B)$ = voltage applied across terminals; $V(S)$ = state variable; r_{on} = low resistance; r_{off} = high resistance	Calculates G_1 based on parameters and variables related to T, B, S, and constants.

3.3. Extraction of Hysteresis Loop-Based Parameters

Figure 3b represents the extraction methods of hysteresis loop-based parameters such as V_p, H_p, V_n, and H_n for the I–V characteristics of different values of the constant (k), positive integers (pi), and initial state variable (x_0). Here, V_p and H_p represent the vertical and horizontal coordinates for the positive half-cycle, while V_n and H_n denote the vertical and horizontal coordinates for the negative half-cycle. The detailed extraction process of V_p, H_p, V_n, and H_n is given below.

a. Measure the maximum voltage of the pinched hysteresis loop for both the positive and negative half-cycles.
b. Calculate half of the maximum voltage for each cycle.
c. Draw a line that divides the positive and negative parts of the pinched hysteresis loop equally, based on half of the maximum voltage.
d. Select two vertical points from the line drawn between the two half-cycles; these points are referred to as V_p.
e. Determine the midpoint of the two vertical points by dividing $V_p/2$ for each half-cycle.
f. Draw a line between the midpoints of the two vertical positions to calculate H_p for each half-cycle.

Here, V_p and H_p represent the vertical and horizontal coordinates for the positive half-cycle, while V_n and H_n denote the vertical and horizontal coordinates for the negative half-cycle. The detailed extraction process of V_p, H_p, V_n, and H_n is given below.

The constant k is an important parameter in the SPICE subcircuit code for a memristor model because it determines the dynamics of the state variable $V(S)$, which represents the internal state of the memristor. The capacitor C_{int} is used to integrate the time derivative, which determines how the state variable $V(S)$ changes over time. The voltage-controlled current source G_s controls the current flowing into C_{int}. The equation for G_s is given by

$$G_s = \left\{ \frac{k \cdot V(T,B)}{r_{\text{on}} \cdot V(S) + r_{\text{off}} \cdot (1 - V(S))} \times \left[1 - (2 \cdot V(S) - 1)^{2pi}\right] \right\} \quad (7)$$

Here, k acts as a scaling factor for the rate at which the state variable $V(S)$ changes in response to the voltage applied across the memristor terminals.

The window function in the Joglekar memristor model uses the term pi (a positive integer) to regulate how the state variable (memristance) varies when the device is operating. In the Joglekar model, the window function is given by

$$f(x) = 1 - (2x - 1)^{2pi} \tag{8}$$

where pi is a positive integer that affects the function's shape and x is the normalized state variable, which ranges from 0 to 1.

The memristor's resistance (memristance) is determined by its internal state variable x_0, which is described by the Joglekar memristor model. The initial state variable x_0, which has a major impact on the electrical properties of the device, is the initial value of x at time $t = 0$. The differential equation that describes how the state variable x changes is

$$\frac{dx}{dt} = k \cdot I(t) \cdot f(x) \tag{9}$$

where x is the normalized state variable ($0 \leq x \leq 1$), k is a constant, $I(t)$ is the applied current, and $f(x)$ is the Joglekar window function.

4. Results and Discussion

This section presents the key findings of the study and discusses their implications. The results are analyzed in comparison to existing models and methodologies, highlighting the advantages of the proposed approach. Additionally, a comparative table summarizing the key parameters obtained in this work alongside recent related studies is presented.

4.1. Calibration of SPICE Simulation Framework

This section presents results on the SPICE framework for egg albumin memristors, including the significant parameters used to represent egg albumin memristors in the SPICE framework. The SPICE model developed has been compared with the experimental results, as shown in Figure 4 in the logarithmic plot. Table 3 presents the various parameters used in the SPICE simulations, tuned to accurately represent an egg albumin memristor. As observed, the developed SPICE model fits closely with the experimental results, demonstrating the accuracy of the developed model.

Table 3. SPICE model parameters (Figure 4) used for simulating egg albumin memristors [40].

SPICE Parameter	SPICE Parameter Value	Parameter Description
r_{off}	2899	Low-resistance state
r_{on}	782	High-resistance state
k	800	Constant
pi	1	Positive integer
x_0	0.906	Initial state variable

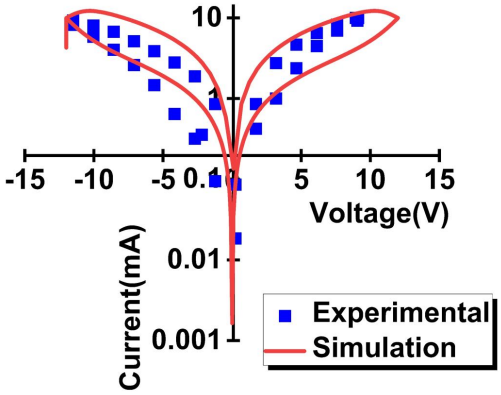

Figure 4. I−V characteristics showing experimental results calibrated with the SPICE model.

The voltage–time plot across the memristor for a constant (k), as well as a voltage–time curve across the memristor for a positive integer (pi) and initial state variable (x_0), is shown in Figure 5. These parameters govern the resistance (or conductance) of the memristor at any given position.

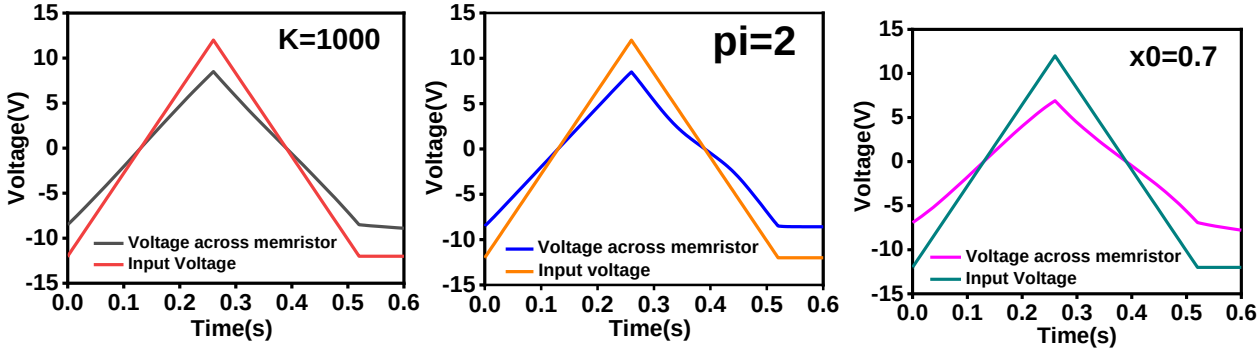

(**a**) (**b**) (**c**)

Figure 5. The voltage−time characteristics for V_m (voltage across the memristor) and V_1 (input voltage) are illustrated for three cases: (**a**) constant (k); (**b**) positive integer (p_i); and (**c**) the initial state variable (x_0).

Based on the voltage sweep on the SMU for the experimental characteristics, a triangular pulse is applied to the circuit with a time of 0.526 s and rise and fall time of 0.26 s. A 1 kΩ resistor is connected in series with it to visualize the voltage drop across the memristor.

4.2. Analysis of Key Parameters of the Calibrated SPICE Model

The I–V characteristics for different constants (k) are shown in Figure 6. The plots indicate that loop widths increase as the value of 'k' increases. Figure 7 displays the extracted graphs of V_p, V_n and H_p, H_n, showing a consistent increase with higher constant (k) values.

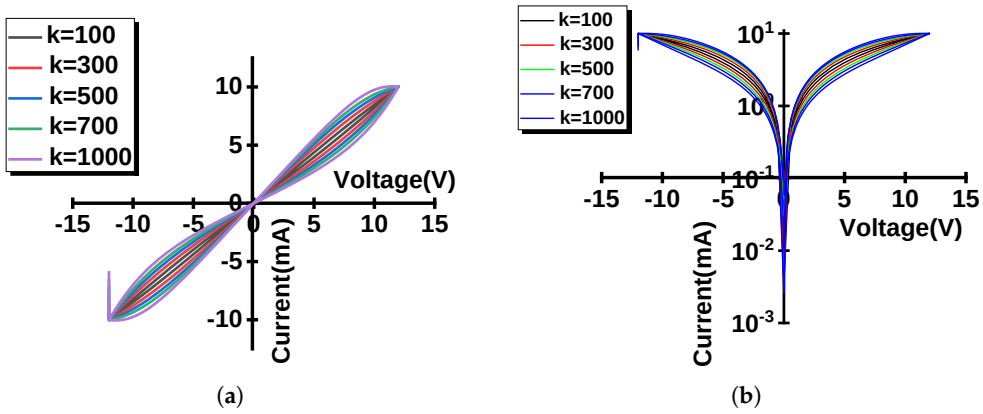

Figure 6. SPICE simulation of experimental data−calibrated egg albumin memristor model for different constants (k) on (**a**) linear scale and (**b**) logarithmic scale.

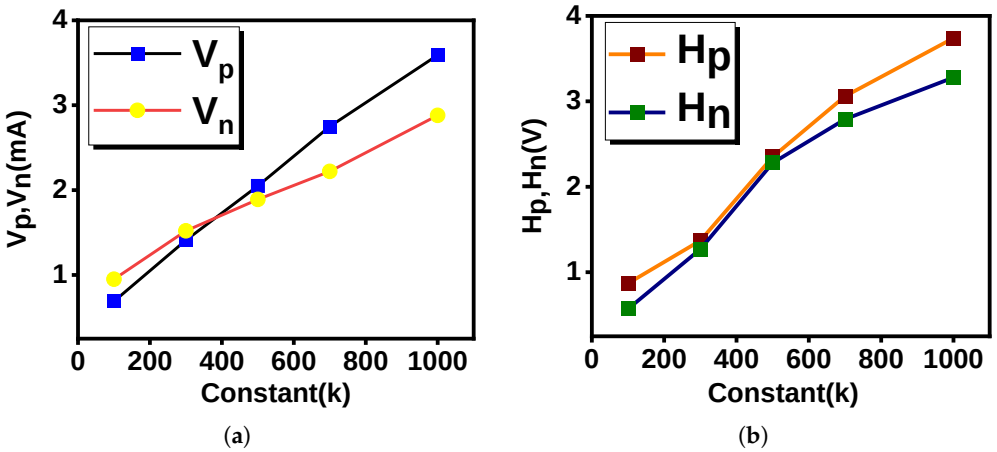

Figure 7. (**a**) Extracted V_P, V_n and (**b**) extracted H_P, H_n for different values of constant (k).

The width of the hysteresis loop increases with k because quicker state development allows for more resistance change within each cycle, resulting in higher voltage swings. However, the actual loop width is also determined by the material properties (such as ion mobility and defect density) and device design (such as thickness and electrode materials), all of which impact how quickly resistance varies in physical devices.

The memristor's resistance (memristance) is determined by its internal state variable x_0, which is described by the Joglekar memristor model. The initial state variable x_0, which has a major impact on the electrical properties of the device, is the initial value of x at time $t = 0$.

The memristor I–V characteristics for different values of the parameter positive integer (pi) are plotted in Figure 8. The values of V_P and H_p increase as the positive integer value (pi) increases. This implies increases in the current and voltage in both the positive and negative half-cycles. Figure 9 shows the extracted graphs of V_p, V_n and H_p, H_n for different positive integers (pi).

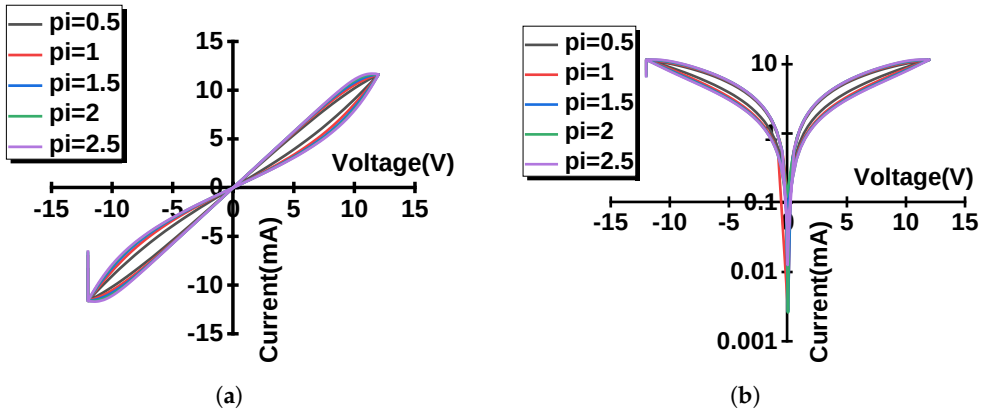

Figure 8. SPICE simulation of experimental data−calibrated egg albumin memristor model for different positive integers (*pi*) on (**a**) linear scale (**b**) logarithmic scale.

The initial state variable is often the variable that reflects the device's status before it begins operating. This state variable is frequently associated with internal memristor features, such as ion dispersion or material flaws. Figure 10 displays the I–V characteristics of the simulation model with varying values of the initial state variable (x_0). As shown in Figure 11, as we vary the initial state-variable values, V_p, V_n, and H_p are observed to increase. Table 4 presents a comparative analysis of previously reported studies with this work. Readers can refer to Supplementary Materials provided in this work for more details.

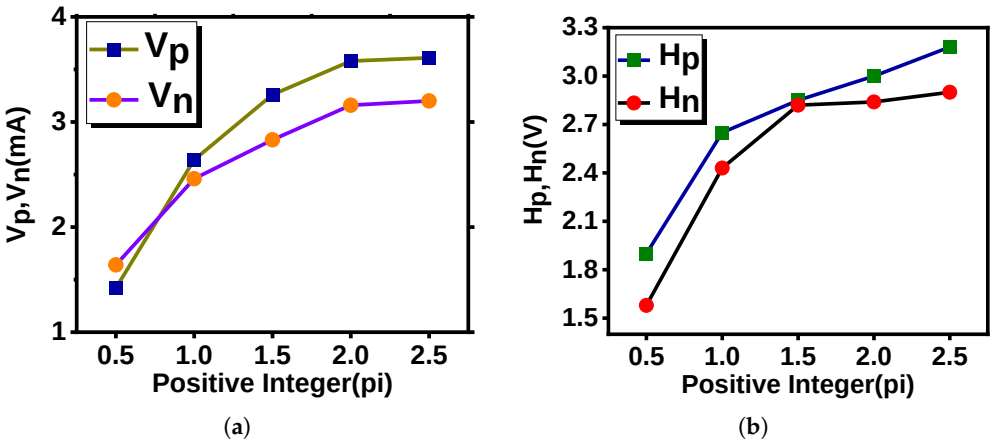

Figure 9. (**a**) Extracted V_P, V_n. (**b**) Extracted H_P, H_n for different values of positive integer (*pi*).

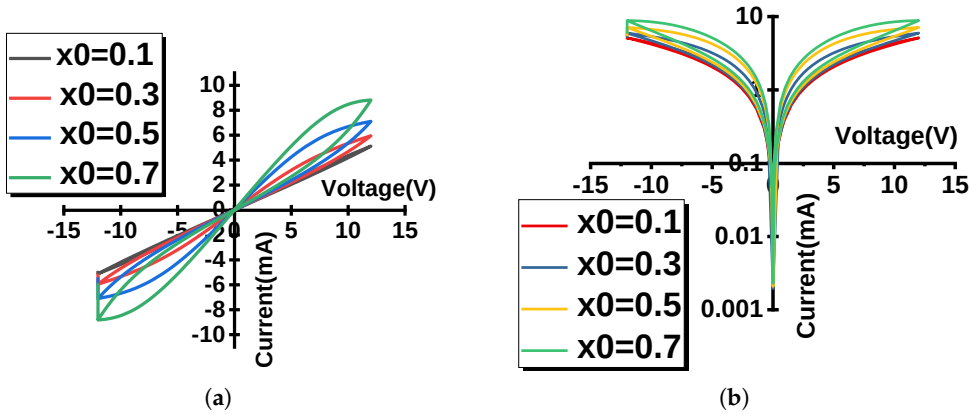

Figure 10. SPICE simulation of experimental data−calibrated egg albumin memristor model for different initial state variables (*x*0) on (**a**) linear scale and (**b**) logarithmic scale.

Table 4. Memristor models for different materials along with the important model parameters and simulation platform.

Year	Memristive Material	Memristor Model	Parameters	Simulation Platform	Ref.
2009	TiO_2	Biolek	$r_{on} = 1\,k\Omega$, $r_{off} = 100\,k\Omega$, $R_{init} = 80\,k\Omega$, $D = 10\ N$, $uv = 10\ F$, $p = 1$	PSPICE	[40]
2017	TiO_2	Yakopcic	$\eta = 1$, $x_0 = 0.11$, $x_p = 0.35$, $x_n = 0.55$, $\alpha_p = 1$, $\alpha_n = 5$, $V_p = 0.1$, $V_n = 0.1$, $A_p = A_n = 4 \times 10^3$, $b = 2 \times 10^{-5}$, $a_1 = a_2 = 17 \times 10^5$	PSPICE	[45]
2017	TiO_2	Pickett	$f_{off} = 3.5\,\mu A$, $i_{off} = 115\,\mu A$, $a_{off} = 1.2$, $f_{on} = 40\,\mu A$, $i_{on} = 8.9\,\mu A$, $a_{on} = 1.8$, $b = 500\,\mu A$, $w_c = 107\,mV$, $k_1 = 11.3153$, $k_2 = 44.6944\,\mu$, $k_3 = 1.34192$, $k_4 = 3.0364$, $k_5 = 11.4919\,n$, $k_6 = 24.1384$, $R_s = 232.047\,\Omega$	CADENCE 16.6	[46]
2024	rGO-CdS nanocomposites	Thang Hoang	$r_{on} = 753\,\Omega$, $r_{off} = 1325\,\Omega$, $T = 300\,K$, MEF = 1.76	MATLAB	[47]
2024	Egg albumin	Joglekar	$r_{on} = 869\,\Omega$, $r_{off} = 2508\,\Omega$, $k = 0.8 \times 10^3$, $pi = 1$, $x_0 = 0.906$	LTSPICE 24.1.3	This work

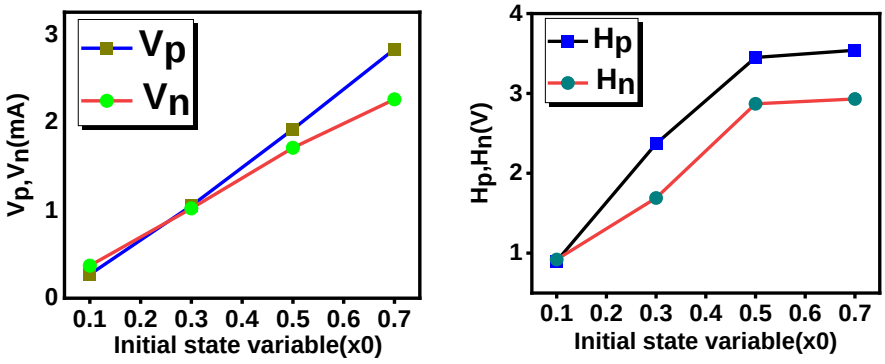

(**a**) (**b**)

Figure 11. (**a**) Extracted V_P, V_n and (**b**) extracted H_P, H_n for different values of initial state variable (x_0).

5. Conclusions and Future Scope

This study calibrated a SPICE simulation model using experimental data from egg albumin memristors fabricated on 3D substrates. The calibrated model was used to analyze key parameters, including the constant k, positive integer, and initial state variable. The significant findings indicate that Joglekar memristor mathematics can effectively represent bio-memristors, such as egg albumin-based memristors. Additionally, the constant k is found to be a crucial parameter in the Joglekar memristor model, while the initial state variable x_0 plays a vital role in calculating the I–V loop area. The presented subcircuit facilitates the development of memristor crossbar array models, enabling the study of important challenges such as sneak paths. Furthermore, using the SPICE model, similar conclusions can be drawn for other organic material-based memristors. Strategies can be developed to incorporate mathematical models that capture slight changes in resistance

states across different cycles. The design and assembly of crossbar arrays for neuromorphic computing circuits represent a promising area for future research.

Supplementary Materials: The following supporting information can be downloaded at: https://www.mdpi.com/article/10.3390/electronics14050838/s1, Figure S1: I-V characteristics of duck egg albumin memristor for 40 cycles (a) Device1; (b) Device2. Figure S2: Resistance state of parameter (a) Constant (k); (b) Positive integer (pi); (c) Initial state variable (x_0).

Author Contributions: Conceptualization, R.G.; Methodology, H.C. and R.G.; Software, H.C.; Validation, H.C.; Formal analysis, H.C.; Investigation, P.K.G. and R.G.; Resources, J.V.; Data curation, H.C., P.K.G. and R.v.d.K.; Writing—original draft, H.C.; Writing—review & editing, P.K.G., R.v.d.K., R.G. and J.V.; Visualization, P.K.G.; Supervision, R.G. and J.V.; Project administration, R.G.; Funding acquisition, R.G. All authors have read and agreed to the published version of the manuscript.

Funding: The authors would like to acknowledge the DST-FIST-sponsored laboratory at the Department of Electronics and Communication Engineering, Tezpur University (Grant No. SR/FST/ET-II/2018/241), for providing the I–V measurement unit. The authors also extend their gratitude to Delft University of Technology for covering the APC charges

Data Availability Statement: The raw data supporting the conclusions of this article will be made available by the authors on request.

Acknowledgments: The authors would like to acknowledge Ayan Sharma for his assistance in building the LaTeX file.

Conflicts of Interest: The authors declare that they have no conflicts of interest.

Appendix A. Memristor SPICE Model

This appendix presents the SPICE model for a memristor, based on the work of Joglekar et al. [30]. The model parameters and circuit elements are described below.

```
.subckt Memristor T B S

*Memristor Parameters:
.params ron=782 roff=2899 k=0.8e3 pi=1 x0=0.906

*Capacitor for integrating the state variable time derivative:
Cint S 0 {1}
.IC V(S)=x0

*High-valued resistance for preventing convergence problems:
Rad S 0 10G

*Memristor state modeling:
Gs 0 S value={(k*V(T,B)*(1/(ron*(V(S))+roff*(1-V(S))))

*(1-pow((2*(V(S))-1),(2*pi))))}

*Memristor conductance:
G1 T B value={V(T,B)*((1/(ron*(V(S))+roff*(1-V(S)))))}

.ends Memristor
```

References

1. Zhu, Y.; Mao, H.; Zhu, Y.; Wang, X.; Fu, C.; Ke, S.; Wan, C.; Wan, Q. CMOS-compatible neuromorphic devices for neuromorphic perception and computing: A review. *Int. J. Extrem. Manuf.* **2023**, *5*, 042010. [CrossRef]
2. Lai, Y.L.; Chiang, W.J. Characteristics of System in a Package of Synchronous Dynamic Random Access Memory for High-Speed Data Storage Applications. *IEEE Trans. Magn.* **2014**, *50*, 1–5. [CrossRef]
3. Jooq, M.K.Q.; Moaiyeri, M.H.; Al-Shidaifat, A.; Song, H. Ultra-Efficient and Robust Auto-Nonvolatile Schmitt Trigger-Based Latch Design Using Ferroelectric CNTFET Technology. *IEEE Trans. Ultrason. Ferroelectr. Freq. Control* **2022**, *69*, 1829–1840. [CrossRef] [PubMed]
4. Rafiq, M.; Chauhan, Y.S.; Sahay, S. Efficient Implementation of Mahalanobis Distance on Ferroelectric FinFET Crossbar for Outlier Detection. *IEEE J. Electron Devices Soc.* **2024**, *12*, 516–524. [CrossRef]
5. Cheng, X.L.; Yin, W.; Feng, Z.G.; Liang, T.Y. Simulation on A Novel Ga-doped Phase Change Memory for Next Generation Embedded Non-Volatile Memory Application. In Proceedings of the 2008 IEEE/SEMI Advanced Semiconductor Manufacturing Conference, Cambridge, MA, USA, 5–7 May 2008; pp. 43–48. [CrossRef]
6. Berdan, R.; Lim, C.; Khiat, A.; Papavassiliou, C.; Prodromakis, T. A Memristor SPICE Model Accounting for Volatile Characteristics of Practical ReRAM. *IEEE Electron Device Lett.* **2014**, *35*, 135–137. [CrossRef]
7. Reddy, L.H.; Pande, S.R.; Roy, T.; Vogel, E.M.; Chakravorty, A.; Chakrabarti, B. A SPICE compact model for forming-free, low-power graphene-insulator-graphene ReRAM technology. *Emergent Mater.* **2021**, *4*, 1055–1065. [CrossRef]
8. Du, N.; Schmidt, H.; Polian, I. Low-power emerging memristive designs towards secure hardware systems for applications in internet of things. *Nano Mater. Sci.* **2021**, *3*, 186–204. [CrossRef]
9. Chua, L. Memristor-The missing circuit element. *IEEE Trans. Circuit Theory* **1971**, *18*, 507–519. [CrossRef]
10. Strukov, D.; Snider, G.; Stewart, D.; Williams, S. The Missing Memristor Found. *Nature* **2008**, *453*, 80–83. [CrossRef]
11. He, X.; Zhang, J.; Wang, W.; Xuan, W.; Wang, X.; Zhang, Q.; Smith, C.G.; Luo, J. Transient Resistive Switching Devices Made from Egg Albumen Dielectrics and Dissolvable Electrodes. *ACS Appl. Mater. Interfaces* **2016**, *8*, 10954–10960. [CrossRef]
12. Pabst, O.; Martinsen, Ø.G.; Chua, L. Information can be stored in the human skin memristor which has non-volatile memory. *Sci. Rep.* **2019**, *9*, 19260. [CrossRef] [PubMed]
13. Volkov, A.G.; Reedus, J.; Mitchell, C.M.; Tuckett, C.; Volkova, M.I.; Markin, V.S.; Chua, L. Memory elements in the electrical network of *Mimosa pudica* L. *Plant Signal. Behav.* **2014**, *9*, e982029. [CrossRef] [PubMed]
14. Chua, L. If it's pinched it's a memristor. *Semicond. Sci. Technol.* **2014**, *29*, 104001. [CrossRef]
15. Zhao, E.; Jiang, J.; Liu, G.; Wang, C.; Zhou, C.; Zhang, Z. Organic polymer artificial synapse device based on amylum memristor. *J. Mater. Sci. Mater. Electron.* **2023**, *34*, 1688. [CrossRef]
16. Ho, H.H.D.; Nguyen, N.H.; Nguyen, N.B.; Le, V.K.; Nguyen, N.U.T.; Le Hoang Doan, T.; Nguyen, L.H.T.; Nguyen, T.H.; Pham, N.K. Development of switching memory devices of cellulose fibers from lotus petioles. *J. Mater. Sci. Mater. Electron.* **2024**, *35*, 387. [CrossRef]
17. Sueoka, B.; Hasan Tanim, M.M.; Williams, L.; Xiao, Z.; Seah, Y.Z.; Cheong, K.Y.; Zhao, F. A synaptic memristor based on natural organic honey with neural facilitation. *Org. Electron.* **2022**, *109*, 106622. [CrossRef]
18. Gale, E.; Adamatzky, A.; De Lacy Costello, B. Slime Mould Memristors. *BioNanoScience* **2014**, *5*, 1–8. [CrossRef]
19. Johnsen, G.K. An introduction to the memristor – a valuable circuit element in bioelectricity and bioimpedance. *J. Electr. Bioimpedance* **2012**, *3*, 20–28. [CrossRef]
20. Hota, M.K.; Bera, M.K.; Kundu, B.; Kundu, S.C.; Maiti, C.K. A Natural Silk Fibroin Protein-Based Transparent Bio-Memristor. *Adv. Funct. Mater.* **2012**, *22*, 4493–4499. [CrossRef]
21. Chen, Y.C.; Yu, H.C.; Huang, C.Y.; Chung, W.L.; Wu, S.L.; Su, Y.K. Nonvolatile Bio-Memristor Fabricated with Egg Albumen Film. *Sci. Rep.* **2015**, *5*, 10022. [CrossRef]
22. Bok, C.; Woo, S.; Chaoxing, W.; Park, J.; Kim, T.W. Flexible bio-memristive devices based on chicken egg albumen:Au@SiO2 core-shell nanoparticle nanocomposites. *Sci. Rep.* **2017**, *7*, 12033. [CrossRef] [PubMed]
23. Yan, X.; Li, X.; Zhou, Z.; Zhao, J.; Wang, H.; Wang, J.; Zhang, L.; Ren, D.; Zhang, X.; Chen, J.; et al. Flexible Transparent Organic Artificial Synapse Based on the Tungsten/Egg Albumen/Indium Tin Oxide/Polyethylene Terephthalate Memristor. *ACS Appl. Mater. Interfaces* **2019**, *11*, 18654–18661. [CrossRef] [PubMed]
24. Choudhury, H.; Goswami, R.; Kumar, G.; Kakoty, N.M. Memristors as Prospective Devices for Silicon and Post-Silicon Eras: Theory, Applications and Perspectives. In *Nanoelectronic Devices and Applications*; Lenka, T.R., Nguyen, H.P.T., Eds.; Bentham Science: Singapore, 2024; Chapter 16, pp. 297–334.
25. Vourkas, I.; Batsos, A.; Sirakoulis, G.C. SPICE modeling of nonlinear memristive behavior. *Int. J. Circuit Theory Appl.* **2015**, *43*, 553–565. [CrossRef]
26. Li, H.; Huang, P.; Gao, B.; Chen, B.; Liu, X.; Kang, J. A SPICE Model of Resistive Random Access Memory for Large-Scale Memory Array Simulation. *IEEE Electron Device Lett.* **2014**, *35*, 211–213. [CrossRef]

27. Yakopcic, C.; Taha, T.M.; Subramanyam, G.; Pino, R.E. Generalized Memristive Device SPICE Model and its Application in Circuit Design. *IEEE Trans. Comput.-Aided Des. Integr. Circuits Syst.* **2013**, *32*, 1201–1214. [CrossRef]
28. Li, B.; Shi, G. A Native SPICE Implementation of Memristor Models for Simulation of Neuromorphic Analog Signal Processing Circuits. *ACM Trans. Des. Autom. Electron. Syst.* **2021**, *27*, 1–24. [CrossRef]
29. Kim, S.; Kim, H.D.; Choi, S.J. Compact Two-State-Variable Second-Order Memristor Model. *Small* **2016**, *12*, 3320–3326. [CrossRef]
30. Joglekar, Y.N.; Wolf, S.J. The elusive memristor: Properties of basic electrical circuits. *Eur. J. Phys.* **2009**, *30*, 661. [CrossRef]
31. Yakopcic, C.; Taha, T.; Subramanyam, G.; Pino, R. Memristor SPICE Modeling. In *Advances in Neuromorphic Memristor Science and Applications*; Springer: Dordrecht, The Netherlands, 2012; pp. 211–244. [CrossRef]
32. Biolek, D.; Biolek, Z.; Biolková, V. PSPICE Modeling of Meminductor. *Analog. Integr. Circuits Signal Process.* **2011**, *66*, 129–137. [CrossRef]
33. Martinsen, Ø.G.; Grimnes, S.; Lütken, C.A.; Johnsen, G.K. Memristance in human skin. *J. Phys. Conf. Ser.* **2010**, *224*, 012071. [CrossRef]
34. Volkov, A.G.; Tucket, C.; Reedus, J.; Volkova, M.I.; Markin, V.S.; Chua, L. Memristors in plants. *Plant Signal. Behav.* **2014**, *9*, e28152. [CrossRef] [PubMed]
35. Volkov, A.G.; Nyasani, E.K.; Blockmon, A.L.; Volkova, M.I. Memristors: Memory elements in potato tubers. *Plant Signal. Behav.* **2015**, *10*, e1071750. [CrossRef] [PubMed]
36. Volkov, A.G.; Nyasani, E.K.; Tuckett, C.; Greeman, E.A.; Markin, V.S. Electrophysiology of pumpkin seeds: Memristors in vivo. *Plant Signal. Behav.* **2016**, *11*, e1151600. [CrossRef] [PubMed]
37. Goswami, R.; Deb, A.; Rathi, R.D.; Mahajan, P. Design and Analyses of a Food Protein Sensing System Based on Memristive Properties. In *Electrical and Electronic Devices, Circuits, and Materials*; John Wiley & Sons, Ltd.: Hoboken, NJ, USA, 2021; Chapter 6, pp. 101–118. [CrossRef]
38. Qin, J.; Sun, B.; Zhou, Y.; Du, J.; Cao, Z.; Mao, S.; Yang, Y.; Liu, M.; Rao, Z.; Ke, C.; et al. Evolution between RS and NRS behaviors in BiFeO3@egg albumen nanocomposite based memristor. *Curr. Appl. Phys.* **2024**, *59*, 77–84. [CrossRef]
39. Ostrovskii, V.; Fedoseev, P.; Bobrova, Y.; Butusov, D. Structural and parametric identification of known memristors. *Nanomaterials* **2021**, *12*, 63. [CrossRef]
40. Biolek, Z.; Biolek, D.; Biolkova, V. SPICE Model of Memristor with Nonlinear Dopant Drift. *Radioengineering* **2009**, *18*, 210–214.
41. Gao, L.; Ren, Q.; Sun, J.; Han, S.T.; Zhou, Y. Memristor modeling: Challenges in theories, simulations, and device variability. *J. Mater. Chem. C* **2021**, *9*, 16859–16884. [CrossRef]
42. Corinto, F.; Ascoli, A. A Boundary Condition-Based Approach to the Modeling of Memristor Nanostructures. *IEEE Trans. Circuits Syst. I Regul. Pap.* **2012**, *59*, 2713–2726. [CrossRef]
43. Ascoli, A.; Tetzlaff, R.; Biolek, Z.; Kolka, Z.; Biolkovà, V.; Biolek, D. The Art of Finding Accurate Memristor Model Solutions. *IEEE J. Emerg. Sel. Top. Circuits Syst.* **2015**, *5*, 133–142. [CrossRef]
44. Biolek, D.; Biolek, Z. Fourth Fundamental Circuit Element: SPICE Modeling and Simulation. In *Memristors and Memristive Systems*; Tetzlaff, R., Ed.; Springer: New York, NY, USA, 2014; pp. 105–162. [CrossRef]
45. Ouaja Rziga, F.; Mbarek, K.; Ghedira, S.; Besbes, K. The basic I–V characteristics of memristor model: Simulation and analysis. *Appl. Phys. A Mater. Sci. Process.* **2017**, *123*, 288. [CrossRef]
46. Biolek, D.; Biolkova, V.; Kolka, Z. Modified MIM model of titanium dioxide memristor for reliable simulations in SPICE. In Proceedings of the 2017 14th International Conference on Synthesis, Modeling, Analysis and Simulation Methods and Applications to Circuit Design (SMACD), Taormina, Italy, 12–15 June 2017; IEEE: New York, NY, USA, 2017.
47. Kalita, A.J.; Sharma, M.; Das, H.; Kalita, P.K. Memristive behaviour of Al/rGO-CdS/FTO device at different temperatures: A MATLAB-integrated study. *Phys. E Low Dimens. Syst. Nanostruct.* **2025**, *165*, 116107. [CrossRef]